Proceedings of the International Conference on Heat Transfer and Fluid Flow
Prague, Czech Republic, August 11-12, 2014
Paper No. 191

Mathematical Modelling of Transient Response of Plate Fin and Tube Heat Exchanger

Anna Korzeń
Cracow University of Technology, Institute of Thermal Power Engineering
al. Jana Pawła II 37, 31-864 Cracow, Poland
korzen@mech.pk.edu.pl

Dawid Taler
Cracow University of Technology, Institute of Thermal Engineering and Air Protection
ul. Warszawska 24, 31-155 Cracow, Poland
dtaler@pk.edu.pl

Abstract - Cross-flow tubular heat exchangers are applied as condensers and evaporators in air conditioners and heat pumps or as air heaters in heating systems. They are also applied as water coolers in so called 'dry' water cooling systems of power plants, as well as car radiators. There are analytical and numerical mathematical models of heat exchangers of that type to determine the steady state temperature distribution of fluids and the rate of heat transferred between fluids. In view of the wide range of applications in practice, these heat exchangers were experimentally examined in steady-state conditions, mostly to determine the overall heat transfer coefficient or the correlation for the heat transfer coefficients on the air side and on the internal surface of the tubes. There exist many references on the transient response of heat exchangers. Most of them, however, focus on the non-steady-state heat transfer processes in parallel and counter flow heat exchangers. In this paper, the new equation set describing transient heat transfer process in tube and fin cross-flow tube exchanger will be given and subsequently solved using the finite volume method.

Keywords**:** Tube and plate-fin heat exchanger, Transient response, Plate-fin mathematical model, Experimental validation.

1. Introduction

In contrast to the existing methods for modelling transient response of heat exchangers with extended surfaces, in which the weighted steady-state heat transfer coefficient on the finned tube side is used, the transient temperature distribution will be calculated in each fins)Smith, 1997; Roetzel, Xuan 1998; Taler, 2009). This allows for computing more exactly the heat flow rate from the fins to the flowing gas. The axial heat conduction in the tube wall will be also accounted for. Transient temperature distributions in continuous fins attached to oval tubes will be calculated using the finite volume – finite element method (Taler, Korzeń 2011a; Taler, Korzeń 2011b). A system of differential equations of the first order for transient temperature at the nodes will be solved using the explicit finite difference method. The developed method for the determining transient temperature distributions in fins is used in the transient analysis of compact heat exchangers to calculate correctly the heat flow rate transferred from the finned surface to the fluid. A transient response of the cross-flow tube and fin heat exchangers is analyzed. Transient equations for both hot and cold fluid are solved using the finite volume method. A mathematical model of a car radiator will be developed and examined experimentally. The automotive radiator for the spark-ignition combustion engine with a cubic capacity of 1580 cm3 is a double-row, two-pass plate-finned heat exchanger. The radiator consists of aluminium tubes of oval cross-section. The cooling liquid flows in parallel through both tube rows. A transient response of the tube and plate fin heat exchanger due to step change of air temperature will be modeled using the developed method. The

numerical model was validated by comparison of outlet water and air temperatures obtained from the numerical simulation with the experimental data. Good agreement between the numerical predictions and experimental results has been found.

2. Mathematical Model of One-row Heat Exchanger

A numerical model of a cross flow tubular heat exchanger, in which air flows transversally through a row of tubes (Fig. 1) will be presented. The system of partial differential equations describing the space and time changes of: liquid T1, tube wall Tw, and air T2 temperatures are, respectively

$$\frac{1}{N_1}\frac{\partial T_1}{\partial x^+}+\tau_1\frac{\partial T_1}{\partial t}=-\left(T_1-T_w\right), \tag{1}$$

$$U_m\delta_w\rho_w c_w\frac{\partial T_w}{\partial t}+\frac{m_f c_f}{s}\frac{\partial \overline{T}_f}{\partial t}=\frac{k_w U_m\delta_w}{L_{ch}^2}\frac{\partial^2 T_w}{\partial\left(x^+\right)^2}+h_w U_w\left(T_1-T_w\right)+h_o U_z\left(\overline{T}_2-T_w\right), \tag{2}$$

$$\frac{1}{N_2}\frac{\partial T_2}{\partial y^+}+\tau_2\frac{\partial T_2}{\partial t}=T_w-T_2, \tag{3}$$

where $\overline{T}_2$ denotes the mean air temperature over the row thickness, defined as

$$\overline{T}_2\left(x^+,t\right)=\int_0^1 T_2\left(x^+,y^+,t\right)dy^+. \tag{4}$$

The symbols $x^+=x/L_{ch}$ and $y^+=y/p_2$ in equations (1-3) stand for dimensionless coordinates.
The numbers of heat transfer units N_1 and N_2 are given by

$$N_1=\frac{h_1 A_{wrg}}{\dot{m}_1 c_{p1}}, \qquad N_2=\frac{h_2 A_{zrg}}{\dot{m}_2 c_{p2}}, \tag{5}$$

where: $s=L_{ch}/n_f$, $A_{wrg}=n_r U_w L_{ch}$, $A_{zrg}=n_r U_z L_{ch}$.

The time constants τ_1 and τ_2 are $\tau_1=\dfrac{m_1 c_{p1}}{h_1 A_{wrg}}$, $\tau_2=\dfrac{m_2 c_{p2}}{h_2 A_{zrg}}$. (6)

The symbols in equations (1-6) denote:

$$m_1=n_r A_w L_{ch}\rho_1,\ m_2=n_r\left(p_1 p_2-A_{oval}\right)\left(s-\delta_f\right)n_f\rho_2, \qquad m_w=n_r U_m\delta_w L_{ch}\rho_w$$
$$m_f=\left(p_1 p_2-A_{oval}\right)\delta_f\rho_w,\ A_w=\pi a b,\ A_{oval}=\pi(a+\delta_w)(b+\delta_w),U_m=\left(U_w+U_z\right)/2.$$

The subscript *w* refers to the wall, *f* to the fin, and *m* to the mean value.
The weighted heat transfer coefficient h_o is defined by

$$h_o(t) = h_2(t)\left[\frac{A_{mf}}{A_{zrg}} + \frac{A_f}{A_{zrg}} \cdot \eta_f(h_2, t)\right]. \quad (7)$$

The initial temperatures of both fluids are equal and amount to T_0. The initial conditions are

$$T_1(x^+, t)|_{t=0} = T_{1,0}(x^+) \ (8), \quad T_w(x^+, t)|_{t=0} = T_{w,0}(x^+) \ (9), \quad T_2(x^+, y^+, t)|_{t=0} = T_{2,0}(x^+, y^+) \ (10)$$

The boundary conditions have the following form

$$T_1(x^+, t)\Big|_{x^+=0} = f_1(t) \quad (11)$$

$$T_2(x^+, y^+, t)\Big|_{y^+=0} = f_2(t) \quad (12)$$

$$\left.\frac{\partial T_w}{\partial x}\right|_{x=0} = 0 \quad (13)$$

$$\left.\frac{\partial T_w}{\partial x}\right|_{x=L_{ch}} = 0 \quad (14)$$

where and are functions of time describing the variation of the inlet liquid temperature and inlet air temperature. The initial boundary problem formulated above (1–14) applies to heat exchangers made of bare tubes and also from finned ones. For bare tubes mf is equal to zero.

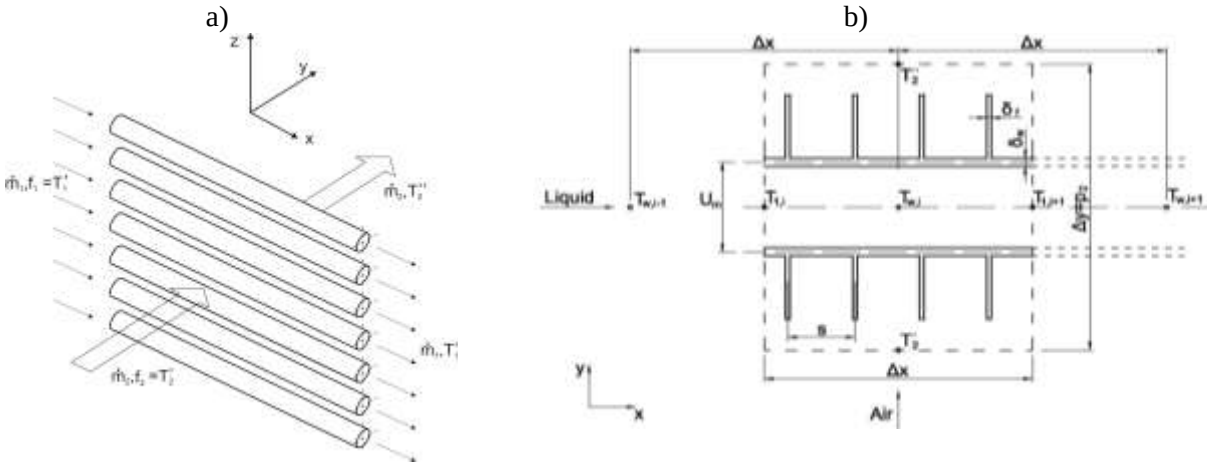

Fig. 1. Scheme of the analyzed heat exchanger (a) and control volume (b).

The transient fluids and tube wall temperature distributions in the one-row heat exchanger (Fig. 1) will be determined by the explicit finite difference method. To calculate time dependent efficiency ηf of the rectangular fin attached to an oval tube the finite volume – finite element method will be used.

2. 1. Finite Difference Model of the Heat Exchanger

When actual heat exchangers are calculated, the thermo-physical properties of the fluids and the heat transfer coefficients depend on the temperature of the fluid, and the initial boundary problem (1-14) is a

non-linear one. In such cases the Laplace transform cannot be applied. The temperature distribution $T_1(x^+, t)$, $T_w(x^+,t)$, and $T_2(x^+, y^+, t)$ can then be found by the explicit finite difference method. In that method, the time derivative is approximated by a forward difference, while the spatial derivatives are approximated by backward or central finite differences. The equations (1–3) are approximated using the explicit finite difference method as follows (Fig. 1b):

$$\frac{1}{N_1^n}\frac{T_{1,i+1}^n - T_{1,i}^n}{\Delta x^+} + \tau_1 \frac{T_{1,i+1}^{n+1} - T_{1,i+1}^n}{\Delta t} = -\left(\frac{T_{1,i}^n + T_{1,i+1}^n}{2} - T_{w,i}^n\right), \qquad i = 1,...,N \qquad n = 0,1,... \tag{15}$$

$$U_m \delta_w \rho_w c_w \frac{T_{w,i}^{n+1} - T_{w,i}^n}{\Delta t} + \frac{m_f c_f}{s}\left[\frac{\eta_{f,i}^{n+1} T_{w,i}^{n+1} + \left(1-\eta_{f,i}^{n+1}\right)\overline{T}_{2,i}^{n+1}}{\Delta t} - \frac{\eta_{f,i}^{n} T_{w,i}^{n} + \left(1-\eta_{f,i}^{n}\right)\overline{T}_{2,i}^{n}}{\Delta t}\right] =$$
$$= \frac{k_w U_m \delta_w}{L_{ch}^2}\frac{T_{w,i+1}^n - 2T_{w,i}^n + T_{w,i-1}^n}{\left(\Delta x^+\right)^2} + h_{w,i}^n U_w \left(\frac{T_{1,i}^n + T_{1,i+1}^n}{2} - T_{w,i}^n\right) - h_{o,i}^n U_z \left(T_{w,i}^n - \overline{T}_{2,i}^n\right), \tag{16}$$

$i = 1,...,N$, $\qquad n = 0,1,...$

$$\frac{1}{N_2^n}\frac{\left(T_{2,i}^{'}\right)^n - \left(T_{2,i}^{"}\right)^n}{1} + \tau_2^n \frac{\left(T_{2,i}^{"}\right)^{n+1} - \left(T_{2,i}^{"}\right)^n}{\Delta t} = T_{w,i}^n - \frac{\left(T_{2,i}^{'}\right)^n + \left(T_{2,i}^{"}\right)^n}{2},\ i = 1,...,N, \tag{17}$$

where

$$\overline{T}_{2,i}^n = \frac{\left(T_{2,i}^{'}\right)^n + \left(T_{2,i}^{"}\right)^n}{2}, \qquad \overline{T}_{2,i}^{n+1} = \frac{\left(T_{2,i}^{'}\right)^{n+1} + \left(T_{2,i}^{"}\right)^{n+1}}{2} \tag{18}$$

The notation used in Equations (15-18) is illustrated in Fig.1. Since the second derivative in Eq. 2 was approximated by the central difference quotient then imaginary nodes at the ends of the tube are necessary. The boundary conditions (13) and (14) are approximated as follows

$$\frac{T_{w,1} - T_{w,0}}{\Delta x} = 0 \tag{19}$$

$$\frac{T_{w,N+1} - T_{w,N}}{\Delta x} = 0 \tag{20}$$

Solving Eqs (19) and (20) for $T_{w,0}$ and $T_{w,N+1}$ gives

$$T_{w,0} = T_{w,1} \text{ and } T_{w,N+1} = T_{w,N}. \tag{21}$$

Equation (21) is accounted for in Eqs (16) for $i = 1$ and $i = N$. The numbers of nodes are shown in Fig. 2. The notation in Fig. 2 is as follows: $W1(I) = T_{1,i}$, $P1(I) = T_{2,i}^{'}$, $P2(I) = T_{2,i}^{"}$, $R1(I) = T_{w,i}$.

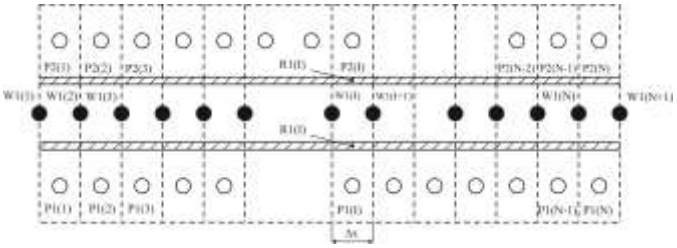

Fig. 2. Finite difference grid used in the calculation of temperature distribution; P1(I) – inlet air temperature, R1(I) – tube wall temperature, P2(I) – outlet air temperature.

The unknown temperature $T_{1,i+1}^{n+1}$ is found from Eq. (15), $T_{w,i}^{n+1}$ from Eq. (16), and $\left(T_{2,i}^{"}\right)^{n+1}$ from Eq. (17):

$$T_{1,i+1}^{n+1}=T_{1,i+1}^{n}-\frac{\Delta t}{N_1^n\,\tau_1^n}\frac{T_{1,i+1}^{n}-T_{1,i}^{n}}{\Delta x^{+}}-\frac{\Delta t}{\tau_1^n}\left(\frac{T_{1,i}^{n}+T_{1,i+1}^{n}}{2}-T_{w,i}^{n}\right),\qquad i=1,...,N,\ \ n=0,1,... \tag{22}$$

$$\begin{aligned}T_{w,i}^{n+1}=T_{w,i}^{n}+\frac{\Delta t}{U_m\delta_w\rho_w c_w+\dfrac{\eta_{f,i}^{n+1}m_f c_f}{s}}\Bigg\{&\frac{k_w U_m\delta_w}{L_{ch}^2}\frac{T_{w,i+1}^{n}-2T_{w,i}^{n}+T_{w,i-1}^{n}}{\left(\Delta x^{+}\right)^2}+h_{w,i}^{n}U_w\left(\frac{T_{1,i}^{n}+T_{1,i+1}^{n}}{2}-T_{w,i}^{n}\right)+\\&+h_{o,i}^{n}U_z\left[\frac{\left(T_{2,i}^{'}\right)^n+\left(T_{2,i}^{"}\right)^n}{2}-T_{w,i}^{n}\right]-\frac{m_f c_f\left(1-\eta_{f,i}^{n}\right)}{s}\frac{\left[\left(T_{2,i}^{'}\right)^{n+1}+\left(T_{2,i}^{"}\right)^{n+1}\right]-\left[\left(T_{2,i}^{'}\right)^{n}+\left(T_{2,i}^{"}\right)^{n}\right]}{2\,\Delta t}\Bigg\}\\&i=1,...,N,\quad n=0,1,...\end{aligned} \tag{23}$$

$$\left(T_{2,i}^{"}\right)^{n+1}=\left(T_{2,i}^{"}\right)^{n}+\frac{\Delta t}{N_2^n\,\tau_2^n}\left[\left(T_{2,i}^{'}\right)^{n}-\left(T_{2,i}^{"}\right)^{n}\right]+\frac{\Delta t}{\tau_2^n}\left[T_{w,i}^{n}-\frac{\left(T_{2,i}^{'}\right)^{n}+\left(T_{2,i}^{"}\right)^{n}}{2}\right],\ i=1,...,N,\ n=0,1,... \tag{24}$$

where $\Delta x^{+}=1/N$.

Equation (23) was derived assuming that $\eta_{f,i}^{n+1}=\eta_{f,i}^{n}$, since the time step Δt is small and the difference between $\eta_{f,i}^{n+1}$ and $\eta_{f,i}^{n}$ is negligible. The initial conditions (8–10) and the boundary conditions (11-12) assume the form:

- initial conditions

$$T_{1,i}^{0}=T_{1,0}\left(x_i^{+}\right),\qquad n=0,\qquad i=1,...,N+1, \tag{25}$$

$$T_{w,i}^{0}=T_{w,0}\left(x_i^{+}\right) \tag{26}$$

$$\left(T_{2,i}^{'}\right)^{0}=T_{2,0}^{'}\left(x_i^{+}\right) \tag{27}$$

$$\left(T_{2,i}^{"}\right)^{0}=T_{2,0}^{"}\left(x_i^{+}\right),\qquad i=1,...,N, \tag{28}$$

where $x_i^{+}=(i-1)\Delta x^{+}$,

- boundary conditions

$$T_{1,1}^{n} = f_1^{n} \tag{29}$$

$$\left(T_{2,i}^{'} \right)^{n} = f_2^{n}, \qquad i = 1,\ldots,N \tag{30}$$

where $f_1^{n} = f_1\left(n\Delta t \right)$, $f_2^{n} = f_2\left(n\Delta t \right)$, $n = 0,1,\ldots$.

In order to ensure stability of the calculations by the explicit finite difference method, the conditions of Courant–Friedrichs–Lewy must be satisfied (Press et al., 2007)

$$\frac{\Delta t}{N_1^{n}\,\tau_1^{n}\,\Delta x^{+}} \le 1, \tag{31}$$

$$\frac{\Delta t}{N_2^{n}\,\tau_2^{n}} \le 1 \tag{32}$$

To avoid numerical diffusion the time step should not be too small (Press et al., 2007). Because of the high air flow velocity w_2, the time step Δt, resulting from the condition (32) should be very small, in the range of tens of thousands of a second. The liquid, air and tube wall temperature distributions are calculated using the formulas (22) and (24) taking into consideration the initial (25-28), the boundary conditions (21), (29-30), starting at n = 0. To compare simulation and measurement results, a simple model of the thermocouple was used to calculate thermocouple response $T_{th}(t)$, when fluid temperature $T_a(t)$ is known from the numerical simulation. The transient response of the thermocouple can be described by a simple differential equation (Jaremkiewicz et al., 2009)

$$\tau_{th}\frac{dT_{th}}{dt} = T_a - T_{th}, \tag{33}$$

where $\tau_{th} = m_{th}\,c_{th} / \left(h_{th}\,A_{th} \right)$ is the time constant of the thermocouple. The symbols in equation (33) are: m_{th} - thermocouple mass, c_{th} - specific heat capacity of the thermocouple, h_{th} - heat transfer coefficient on the surface of the thermocouple, and A_{th} - area of the outside surface of the thermocouple. Approximating the time derivative in Eq. (33) by the central difference quotient and transforming Eq. (33) gives

$$T_a\left(t \right) = T_{th}\left(t \right) + \tau_{th}\frac{T_{th}^{n+1} - T_{th}^{n-1}}{2\,\Delta t_{th}}, \tag{34}$$

where $T_{th}^{n+1} = T_{th}\left(t + \Delta t_{th} \right)$, $T_{th}^{n-1} = T_{th}\left(t - \Delta t_{th} \right)$, and Δt_{th} is the sampling time interval during temperature measurement by means of the data acquisition system. The time constant τ_{th} of the thermocouple is a function of air velocity w_a at the cross section where the air temperature was measured (Jaremkiewicz et al., 2009). This time constant of the thermocouple depends on air velocity and was approximated by the following function

$$\tau_{th} = \frac{1}{0.01617 + 0.02274\sqrt{w_a}}, \tag{35}$$

where the time constant τ_{th} is expressed in s and air velocity w_a in m/s.

2. 2. Modelling of Transient Heat Transfer through Rectangular Fins

The method presented in (Taler, Korzeń 2011a; Taler, Korzeń 2011b) was used to calculate transient temperature distribution in the fins and subsequently time dependent fin efficiencies. Transient temperature distributions in continuous fins attached to oval tubes were calculated using the finite volume – finite element method. The continuous plate fin is broken into the imaginary fins. The imaginary fin model is divided into triangular elements and then finite volumes were formed around the nodes by connecting triangle gravity centres with side centres of triangles (Fig. 3a). After calculating the temperature distribution, the heat transferred from the fin to the environment and fin efficiency will be computed and compared with the results obtained by using the commercial software ANSYS 11.0. The fin was divided into 19 finite volumes (Fig. 3a). The lateral surfaces: 4-19, 1-13, 2-3 are thermally insulated, while on the surfaces:4-6-3 and 1-5-2 convection heat transfer occurs. The computations were carried out for the following data: c = 896 J/(kg·K), ρ = 2707 kg/m^3, k = 207 W/(m·K), δ_f = 0.08 mm, T_f = 0 °C, T_b = 100 °C, T_0 = 0 °C, h = 50 W/(m^2·K).

a) b)

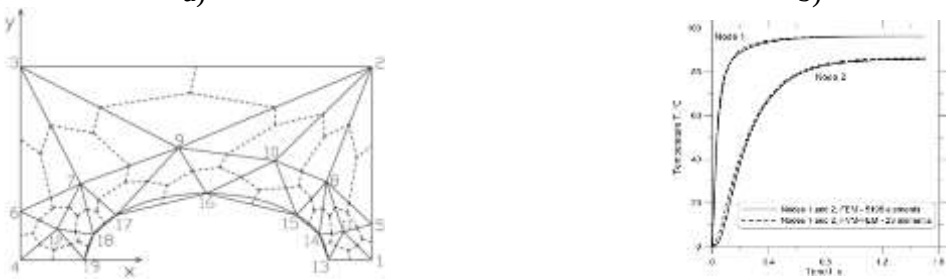

Fig. 3. Fin attached to oval tube (a) and time changes of fin temperature at nodes 1 and 2.

The fin efficiency was also determined based on the temperature distribution obtained by the developed method

$$\eta_{fin} = \frac{\sum_{i=1}^{N} A_{123,i}\left(T_{o,i} - T_f\right) + \sum_{j=1}^{N_l} A_{l,j}\left(\bar{T}_{l,j} - T_f\right)}{A_{fin}\, h\left(T_b - T_f\right)} \quad , \tag{36}$$

where the symbols denote: $A_{123,i}$ – surface area of the ith triangle, $T_{o,i}$ – fin temperature at the gravity center of the ith triangle, N – number of triangles, $A_{l,j}$ – area of the jth lateral surface with the thickness δ_f, $\bar{T}_{l,j}$ – mean temperature of the jth lateral surface with the thickness δ_f , N_l – number of lateral surfaces with the thickness δ_f .The comparison of the fin efficiency calculated from the expressions (36) for the FVM-FEM mesh shown in Fig. 3a and ANSYS results obtained for very fine mesh is presented in Table 1.

Table. 1. Comparison of the fin efficiency obtained using the FVM-FEM (Eq.(36)) and ANSYS software.

h, W/(m^2·K)	0	25	50	75	100	125	150	175
Eq.(36)	1	0.9491	0.9081	0.8712	0.8376	0.8070	0.7789	0.7531
ANSYS	1	0.9502	0.9060	0.8664	0.8308	0.7986	0.7692	0.7424

The accuracy of the present method is very satisfactory. In spite of the coarse finite volume mesh used in present method (Fig. 3a.) the coincidence of the calculated efficiencies is very good. The transient

response of the fin illustrates Fig. 3b. The agreement of the results obtained by the developed method and ANSYS is good. Using the present method for calculating the transient temperature distribution and fin efficiency, the transient heat flow rate transferred from the hot liquid to cold air can be calculated more accurately.

3. The Numerical Model of the Heat Exchanger

The automotive radiator for the spark-ignition combustion engine with a cubic capacity of 1580 cm^3 is a double-row, two-pass plate-finned heat exchanger. The radiator consists of aluminium tubes of oval cross-section. The water flows in parallel through both tube rows. Figure 4a shows a diagram of the two-pass cross-flow radiator with two rows of tubes. The heat exchanger consists of the aluminium tubes of oval cross-section. There are $2n_u$ = 20 tubes in the upper pass, with n_u in the first and second row. Similarly, there are $2n_l$ = 18 tubes in the first and second rows in the lower pass, with n_l in each of them. Mass flow rate of the liquid that passes through the first row of tubes in the upper pass is equal to half of the total $\dot{m}_w$ flow rate (Fig. 4a). Fig. 4b shows the division of the first pass (upper pass) into control volumes. In order to increase the accuracy of the calculations, a staggered mesh was applied. Water temperatures at the control volume nodes are denoted by W1(I) and W2(I) for the first and second rows of tubes, respectively. P1(I) denotes air temperature $T'_{um,i} = T'_{am}(t)$ in front of the radiator, P2(I) denotes the air temperature , $T''_{um,i}$, after the first row of tubes and P3(I) denotes the air temperature, $T'''_{um,i}$, after the second row of tubes in the i-th control volume. Using the notation shown in Fig. 4a the boundary conditions can be written in the following form:

$$W1(1) = W2(1) = T'_w(t) = T'_{w,1}(t) = T'_{w,2}(t), \quad P1(I) = T'_{am}(t) \quad I = 1,...,N. \tag{37}$$

The inlet air velocity, w_0, and mass flow rate, $\dot{m}_w$, are also functions of time. In the simulation program, the time variations of $T'_w(t)$, $T'_{am}(t)$, $w_0(t)$, and $\dot{m}_w(t)$ were interpolated using natural splines of the third degree. The temperature $T_{wm}(t)$ is a temperature of the water at the outlet of the upper pass, where the water of temperature $W1(N+1)$ from the first row of tubes has been mixed with the water of temperature $W2(N+1)$ flowing out of the second row of tubes. In the case of the automotive radiator, temperature $T'_w(t)$ denotes the water temperature at the inlet to the radiator whereas $T'_{am}(t)$ denotes air temperature in front of the radiator.

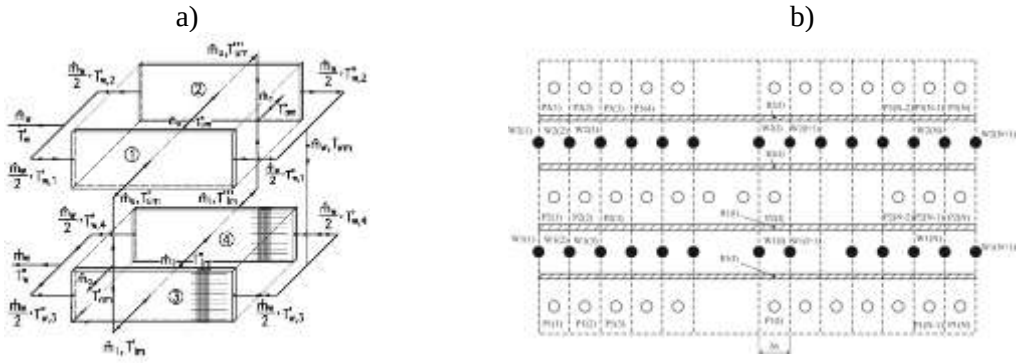

Fig. 4. Flow arrangement of two row cross-flow heat exchanger with two passes (a) and division of the first pass of the car radiator into control volumes (b); 1 – first tube row in upper pass, 2 - second tube row in upper pass, 3 - first tube row in lower pass, 4 - second tube row in lower pass, ○ - air temperature, ● - water temperature.

Having determined the mean temperatures of the air, T'''_{um} and T'''_{lm}, while leaving the second row of tubes in the upper and lower pass, respectively, a mean temperature of the air behind the whole radiator, $T''_{am} = \left(n_u T'''_{um} + n_l T'''_{lm}\right)/n_t$ was calculated. If the water and air temperatures are known, the heat transfer rate in the first and second rows of tubes in the upper and lower passes can be determined. The total heat transfer rate for the radiator was calculated using the formula $\dot{Q}_{chl} = \dot{m}_w\left[i_w\left(T'_w\right) - i_w\left(T''_w\right)\right] = \dot{m}_a \bar{c}_{pa}\left(T''_{am} - T'_{am}\right)$. The numerical model of the heat exchanger described briefly above is used to simulate its transient operation. Before starting transient simulation, the steady-state temperature distribution of water, tube wall and air was calculated using the steady-state mathematical model of the heat exchanger.

4. Experimental Verification

In order to validate the developed model of the heat exchanger, an experimental test stand was built. The measurements were carried out in an open aerodynamic tunnel. The experimental setup was designed to obtain heat transfer and pressure drop data from commercially available automotive radiators. Air is forced through the open-loop wind tunnel by a variable speed axial fan. The air flow passes through the whole front cross-section of the radiator.

A personal computer-based data-acquisition system was used to measure, store and interpret the data. The relative difference between the air-side and liquid-side heat transfer rate was less than 3%.

Extensive heat transfer measurements under steady-state conditions were conducted to find the correlations for the air- and water-side Nusselt numbers, which enable calculation of heat transfer coefficients. Based on 47 measurement series, the following correlations were identified:

$$Nu_w = 0.021\,\mathrm{Re}_w^{0.8038}\,\mathrm{Pr}^{0.3}\left[1+\left(\frac{d_r}{L_{ch}}\right)^{2/3}\right], \qquad 3500 \le \mathrm{Re}_w \le 11000 \tag{38}$$

$$Nu_a = 0.073\,\mathrm{Re}_a^{0.7}\,\mathrm{Pr}_a^{1/3}, \qquad 60 \le \mathrm{Re}_a \le 350 \tag{39}$$

where the symbol d_r stands for the hydraulic diameter of the oval tube.

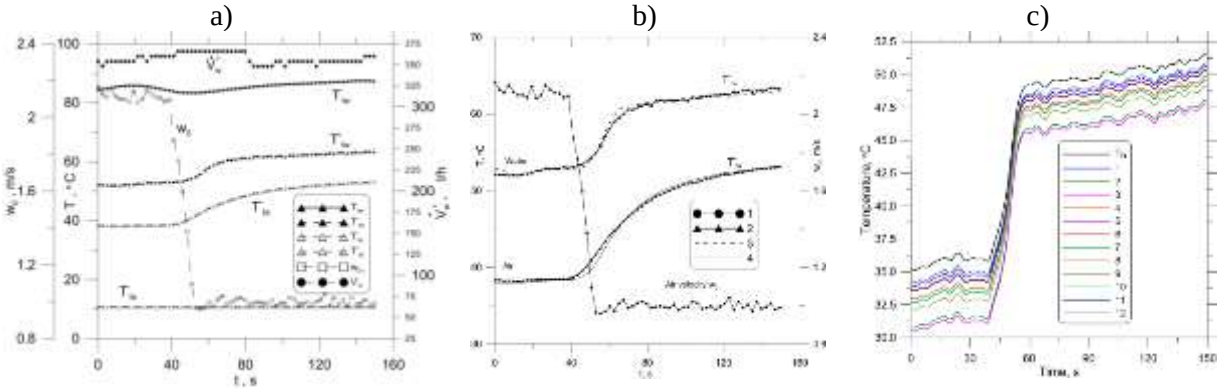

Fig. 5. Time variations of measured data (a), computed outlet water and air temperatures (b) and fin temperature at selective nodes (c); T'_{tw} - water inlet temperature, T'_{ta} - air inlet temperature, T''_{tw} - water outlet temperature, T''_{ta} - air outlet temperature, $\dot{V}'_w$ - water mass flow rate, w_0 - air velocity before the heat exchanger, T_b – fin base temperature, curve numbers in Fig. 5c correspond to node numbers in Fig. 3a.

The water-side Reynolds number $\mathrm{Re}_w = w_w d_r / \nu_w$ is based on the hydraulic diameter $d_r = 4A_w / U_w$, where A_w denotes inside cross section area of the oval tube. The hydraulic diameter for the investigated radiator is: $d_r = 7.06 \cdot 10^{-3}$ m. The air-side Reynolds number is defined as $\mathrm{Re}_a = w_{\max} d_h / \nu_a$, where $w_{\max}$ is mean axial velocity of air in the minimum free flow area, and $d_h = 1.42 \cdot 10^{-3}$ m is the air-side hydraulic diameter. The physical properties of air and water were approximated using simple functions. The effect of temperature-dependent properties is accounted for by evaluating all the properties at the mean temperature of air and water, respectively. Then, the transient response of the heat exchanger was analyzed. Using the measured values of the inlet water temperature, T'_w, the inlet air temperature, T'_{am}, air velocity in front of the radiator, w_0, and the water volumetric flow rate $\dot{V}'_w$, the water, tube wall and air temperatures are determined using the present explicit finite difference method. During the experiment the air inlet velocity was suddenly decreased (Fig. 5a). The calculation results and their comparison with experimental data are shown in Fig. 5b. The agreement between the calculated and measured water and air temperatures at the outlet of the heat exchanger is very good. In the case of water temperature measurement, the time constant of the thermocouple is very small, since the heat transfer coefficient in the thermocouple surface is very high, and the temperature indicated by the thermocouple and the real water temperature are very close.

5. Conclusions

The numerical model of a cross-flow tube heat exchanger, which enables heat transfer simulation under transient conditions was developed. First, the transient temperature distributions of fluids, tube walls and fins in the one row tubular cross flow heat exchanger were determined using the finite difference method. Transient heat transfer through rectangular fins attached to the oval tubes was modeled using the Finite Volume Method – Finite Element Method. Then, the numerical model of the two row heat exchanger with two passes was presented. The numerical model was validated by comparison of outlet water and air temperatures obtained from the numerical simulation with the experimental data. The discrepancy between numerical and experimental results is very small.

References

Jaremkiewicz M., Taler D., Sobota T. (2009). Measuring transient temperature of the medium in power engineering machines and installations, Applied Thermal Engineering, vol. 29, pp. 3374–3379.

Press W.H., Teukolsky S.A., Vettering W.T., Flannery B.P. (2007). Numerical Recipes, The Art of Scientific Computing. Third Edition, Cambridge University Press, Cambridge.

Roetzel W., Xuan Y. (1998). Dynamic behaviour of heat exchangers, Computational Mechanics Publications Vol.3, WIT Press, Southampton.

Smith E. M. (1997). Thermal Design of Heat Exchanger, John Wiley & Sons, Chichester.

Taler D. (2009). Dynamics of Tube Heat Exchangers, Publishing House of AGH University of Science and Technolygy (UNWD), Cracow, (in Polish).

Taler D., Korzeń A. (2011a). Numerical modeling of heat transfer in plate fins, Thermodynamics in Science and Technology, ed. Bogusławski L.,Procedings of the 1-st International Congress on Thermodynamics, Poznań, Poland, Sep. 4-7, pp. 655-664.

Taler D., Korzeń A. (2011b). Modeling of heat transfer in plate fins of complex shape, Rynek Energii, No. 6, 2011, pp. 61-65 (in Polish)